

Experimental investigation of concrete frames reinforced with GFRP bars under reversed cyclic loading

George Hopartean^{*,1}, Ted Donchev^{*,1}, Diana Petkova, Costas Georgopoulos, Mukesh Limbachiya

School of Engineering and Environment, Faculty of Engineering, Computing, and the Environment, Kingston University, 55-59 Penrhyn Rd, Kingston upon Thames, KT1 2EE London, UK

ARTICLE INFO

Keywords:

FRP RC frames
Beam-column joints
GFRP reinforcement
Cyclic loading
Experimental investigation
Seismic behaviour
Earthquake design

ABSTRACT

Fiber reinforced polymers (FRP) have been widely investigated and successfully used as internal reinforcement in new reinforced concrete (RC) members and structures such as slabs, beams, bridges, multi-storey car parks and others as means to overcome the corrosion problem of steel. The linear-elastic behaviour, brittle failure and low modulus of elasticity are some of the significant mechanical characteristics of FRP rebars which raise concerns on their capability to allow structural members to dissipate energy in seismic zones and thus limit their use in earthquake resistant RC structures (such as moment resisting frames). The behaviour of concrete frames reinforced with FRP bars is still in its early stages of research and development with only a few researchers exploring such structures under in-place cyclic loading (seismic loading). As a result, design codes do not provide guidance for RC moment frames internally reinforced with FRP. This study attempts to partially fill the gap by investigating the behaviour of glass fiber reinforced polymers (GFRP) RC frames under in-plane loading. Six 1/3 scaled RC frames were constructed and tested under reversed cyclic loading to simulate seismic loading conditions. Three were reinforced with GFRP bent bars and three (their counterparts) with conventional steel. The testing was conducted in displacement-controlled mode with the loading history according to ACI 374.1–05. Test parameters included longitudinal reinforcement ratio and arrangement in the columns and presence of links in the joints. The experimental results are presented as hysteretic curves, lateral load / drift graphs, stiffness degradation and cumulative energy dissipated with the overall indication of the feasibility of GFRP RC frames in seismic regions. All GFRP specimens successfully reached 2.75% loading drifts. The energy dissipation of GFRP specimens was lower at initial drifts compared to the steel reinforced samples, but it became greater at final drift. GFRP frames had approximately the same load bearing capacity as their counterparts and even greater in one case. Ultimate loads for G frames were reached at higher level of displacement than for S frames.

1. Introduction

It is well known that the corrosion of internal steel reinforcement in reinforced concrete (RC) structures is a major concern in terms of service life of the developments. In almost half a century, many solutions have been studied in order to improve the durability of the structures. As a result, fiber reinforced polymer (FRP) reinforcing bars have been seen by many researchers as a viable alternative to steel in reinforced concrete structures [1–3]. The main characteristics that made the FRP bars the focus of intensive research are their corrosion resistant nature, light weight, high tensile strength and electromagnetic neutrality [4]. In the

last few decades, through extensive laboratory experiments, field applications and implementations, guides, specifications and design codes, FRP bars have gained worldwide acceptance as internal reinforcement in new concrete structures [5–7]. Due to their relatively low cost compared with other FRPs, glass fiber-reinforced polymers (GFRP) have become popular in the construction industry and have been successfully used in bridges, parking garages, water tanks, tunnels and marine structures [8].

The physical and mechanical properties of GFRP rebars and other FRPs in general are different from those of the steel rebars. For instance, GFRP bars have low modulus of elasticity (40–60 GPa compared to the

* Corresponding authors.

E-mail addresses: g.hopartean@kingston.ac.uk (G. Hopartean), t.donchev@kingston.ac.uk (T. Donchev).

¹ Present address Kingston University, London, 55–59 Penrhyn Rd, Kingston upon Thames KT1 2EE.

steel of 200 GPa), which could cause large deformations of the structure. Furthermore, the FRP reinforcement shows linear elastic behaviour without yielding and a brittle failure [9]. This behaviour significantly reduces the ductility of structural elements reinforced with GFRP. In seismic areas, the design philosophy and detailing scheme should be adopted in such a way that the RC structure exhibits adequate ductility, enough to dissipate the energy resulted from seismic activities, thus avoiding catastrophic collapse. Accordingly, the feasibility of using GFRP rebars in seismic regions as a main reinforcement in concrete structures could be considered as questionable. Furthermore, current codes and guidelines for design of the FRP-RC structures such as ACI 440.11–12 [10], fib Model Code 2010 [11] and ACI 440.1R-15 [12] do not provide recommendations and provisions for seismic design of RC frames due to a lack of seismic experiments on earthquake resisting systems reinforced with FRP rebars as main reinforcement. This lack of data and research hinders the use of such materials as sustainable reinforcement for new constructions in seismic zones.

2. Background

Even though many researchers have focused on investigating the behaviour of concrete elements such as slabs, beams and columns reinforced with FRP bars, only very few have explored the behaviour and performance of RC frames (as earthquake resistant systems) internally reinforced with FRP bars under reversed cyclic loading. In an attempt to address this issue and to better understand the behaviour of such structures, in a pioneer experiment by Fukuyama et al. [13], the applicability of FRP bars as main internal reinforcement for concrete frames was investigated. The authors tested under quasi-static loading a half-scale three storey concrete frame reinforced with aramid FRP bars as main and shear reinforcement. The study concluded that earthquake resistant concrete structures reinforced with FRP bars were feasible. After that, a few other researchers have studied the seismic behaviour of GFRP-RC beam-column joints. Said and Nehdi [14] investigated the performance of steel-free GFRP-reinforced beam-column joints. The first specimen (as control sample) was steel-reinforced while the second specimen was GFRP-reinforced. Both specimens were tested under reversed cyclic loading and the results showed that the GFRP-reinforced beam-column joint had lower energy dissipation and lower stiffness than the steel-reinforced beam-column joint but showed a satisfactory drift capacity. Mady et al. [15] investigated the seismic behaviour of four beam-column joints reinforced with GFRP bars and stirrups compared with one specimen reinforced with steel. The experimental results revealed lower energy dissipation and lower stiffness for the GFRP reinforced specimens, but they safely reached drift capacity of 4%, which indicates the feasibility of such joints. In both studies, the GFRP beam-column joints safely resisted lateral displacements up to 3% drift ratio and 4% respectively without exhibiting brittle failure. Also, the cumulative energy dissipated for the steel reinforced specimens was 3 to 4 times greater than for the GFRP reinforced specimens. Likewise, Sharbatdar et al. [16] showed that FRP reinforced joints safely reached drifts of 3% and could be used in new concrete structures.

Subsequently, following these promising results, some researchers investigated the influence of different parameters. For example, the shear capacity of exterior beam column joints reinforced with GFRP bars and stirrups was investigated by Hasaballa and El-Salakawy [17]. The authors suggested that the joint shear stress should be limited. Moreover, similar studies were conducted to evaluate the influence of slabs and lateral beams on exterior beam-column joints. GFRP RC joints confined with lateral beam showed linear behaviour and minimum residual damage up to a drift ratio of 5% [18], while the presence of slabs significantly increased energy dissipation of beam-column connections but did not increase the bending moment capacity of the main beam in compression [19]. A recent study [20] also pointed out that because of the low elastic modulus combined with the high tensile strength of the GFRP bars, concrete elements reinforced with GFRP can be subjected to

significant displacement during an earthquake without exhibiting brittle failure. Another research found that frames reinforced with GFRP bars showed higher strength than frames reinforced with steel bars under seismic loads [21].

Another important parameter which can influence the behaviour of GFRP RC joints is the anchorage type and performance of FRP rebars. The anchorage performance of GFRP headed and bent bars in beam-column joints subjected to seismic loading was investigated by Hasaballa and El-Salakawy [22] and the study concluded that all specimens sustained 4% loading drifts, but the specimens with bent bars sustained higher drift ratios which resulted in higher energy dissipation. High-strength lightweight concrete was also investigated in a beam-column connection reinforced with GFRP [23]. The authors found that the same ratio of glass fiber bars in the beam using high-strength lightweight concrete as opposed to conventional steel reinforcement bars with normal strength concrete enhanced the first cracking load by about 25%.

As most of the studies in the literature are mainly focused on sub-assembly such as beam-column joints, a more global evaluation is needed to better understand the suitability of GFRP reinforced RC frames in seismic areas. So, to date, there is little experimental testing on concrete frames reinforced with FRP bars. Consequently, this paper intends to investigate the seismic behaviour and performance of scaled down GFRP reinforced RC frames under seismic loading compared with their steel reinforced control samples. Six RC frames were constructed and tested under reversed cyclic loading. Test parameters included longitudinal reinforcement ratio and arrangement in the columns and presence of links in the joints.

3. Experimental program

This study investigates the behaviour of concrete frames reinforced with GFRP bars under reversed cyclic loading. The experimental study consists of designing, constructing and testing up to failure under reversed cyclic loading of six 1/3 scaled reinforced concrete frames.

3.1. Test specimens and design details

The specimens were designed to be 1/3 scaled down with the design philosophy of the strong column-weak beam concept. The RC beams and columns were designed according to the EC2 [24] with additional provisions from the EC8 [25] for stirrups arrangements. The GFRP reinforced frames were constructed with the same amount of reinforcement as their counterparts.

Six specimens were constructed in three series. Each series had one control sample, reinforced with conventional steel, and one reinforced with longitudinal GFRP bars and steel stirrups. Table 1 identifies the specimens names along with the longitudinal and transversal reinforcement provided, the links and the actual concrete compressive strength of the samples. The specimens were identified such that the first letter showed if the sample was the control one (reinforced with conventional steel) "S", or if it was the one reinforced with longitudinal GFRP bars, "G". The following digit represents the series that the sample is part of. For example, G2 is the specimen reinforced with longitudinal GFRP bars from Series 2.

All specimens had identical geometry. Fig. 1(a) illustrates the overall concrete dimensions of the specimens which were 1200 mm by 860 mm. The columns measured 860 mm long with a cross section of 120 × 200 mm while the beam length was 1200 mm with a cross section of 120 × 180 mm. The rigid foundation, which measured 1430 mm long, 300 mm wide and 200 mm deep, was cast with the frame in order to provide fixed end conditions at the column bases. The design details of the RC frames (bare frames) are shown in Fig. 1(c).

The cross sections of the samples are showed in Table 2. The first series' specimens (S1 and G1) had eight reinforcement bars in the columns and no links at the joints; the second series (S2 and G2) had six

Table 1
Specimens details.

	Frames ID	Beam reinforcement	Columns reinf	Links in the joint	Concrete Cube compressive strength (MPa)	Standard deviation
Series 1	S1	Top 2 $\varnothing 6$ mm Bottom 2 $\varnothing 6$ mm	8 $\varnothing 6$ mm	No	42	5.57
	G1	T 2 $\varnothing 6$ mm GFRP B 2 $\varnothing 6$ mm GFRP	8 $\varnothing 6$ mm GFRP	No		
Series 2	S2	T 2 $\varnothing 6$ mm B 2 $\varnothing 6$ mm	6 $\varnothing 6$ mm	No	37	2.40
	G2	T 2 $\varnothing 6$ mm GFRP B 2 $\varnothing 6$ mm GFRP	6 $\varnothing 6$ mm GFRP	No		
Series 3	S3	T 2 $\varnothing 6$ mm B 2 $\varnothing 6$ mm	6 $\varnothing 6$ mm	Yes	42	5.33
	G3	T 2 $\varnothing 6$ mm GFRP B 2 $\varnothing 6$ mm GFRP	6 $\varnothing 6$ mm GFRP	Yes		

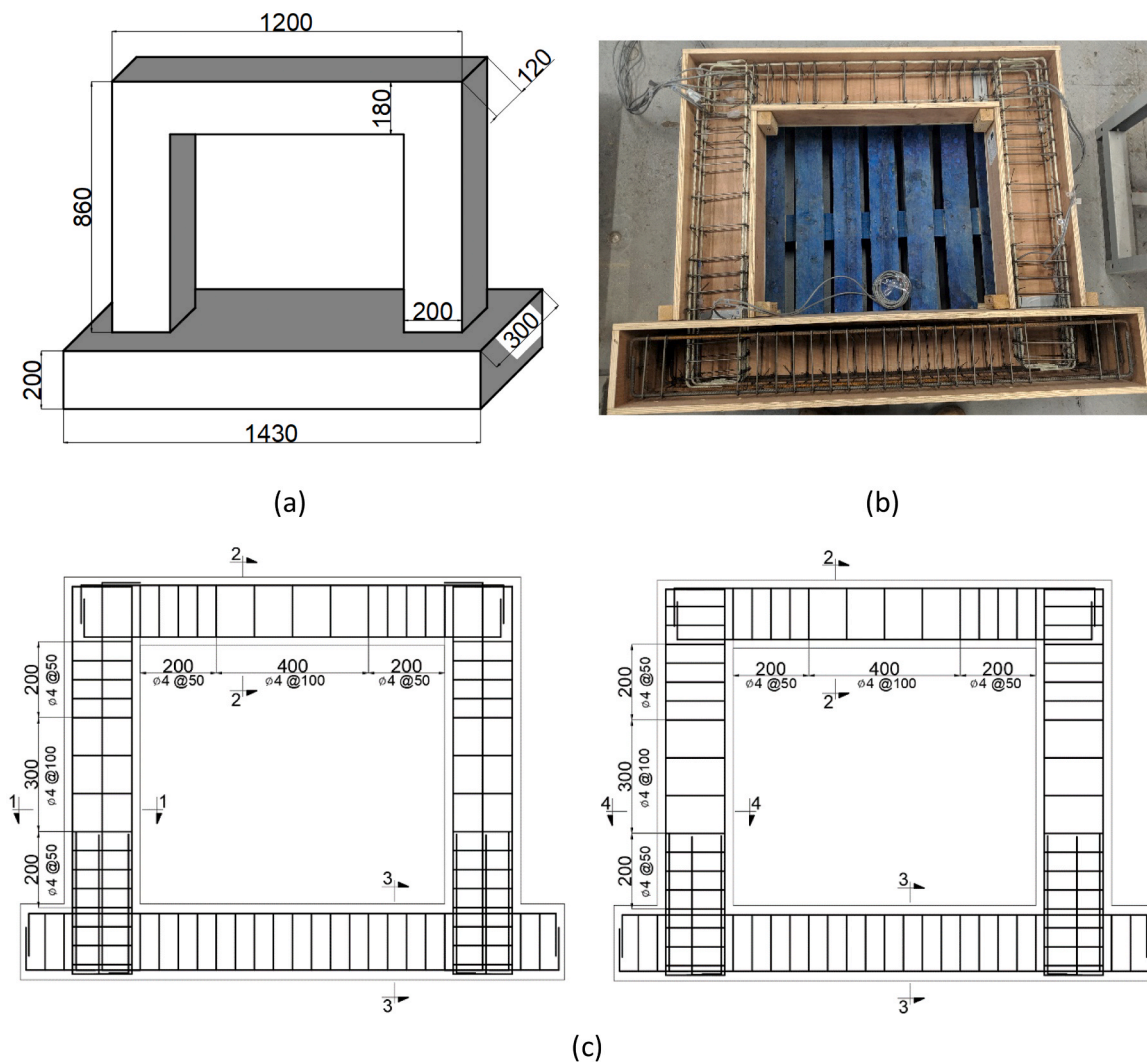


Fig. 1. Details of test specimens: (a) overall dimensions for all specimens, (b) photo of specimens, (c) reinforcement details.

reinforcement bars in the columns and no links in the joints and the third series (S3 and G3) had six reinforcement bars in the columns and links in the joints. Four reinforcement bars were provided for the beams in all the series.

The columns were reinforced with 8 rebars of 6 mm diameter while the beam was reinforced with 4 rebars of 6 mm in diameter. The round mild steel stirrups were 4 mm diameter. For all specimens, the foundations were identical, reinforced with conventional steel bars 8no of

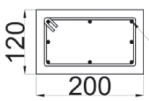
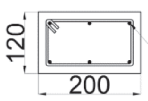
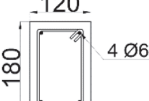
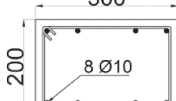
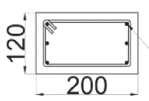
10 mm diameter as to provide fixed-end conditions to the columns and to ensure adequate stiffness and stability is provided to the frame. The anchorage bolts were embedded into the footing and cast along with the frame.

3.2. Material properties

The specimens were constructed (in the laboratory) by using normal

Table 2

Cross sections and reinforcement details for all samples.

Specimens S1,G1	Specimens S2,G2	Specimens S1,S2,S3,G1,G2, G3	Specimens S1,S2,S3,G1,G2,G3	Specimens S3, G3
				
Section 1-1	Section 1-1	Section 2-2	Section 3-3	Section 4-4

concrete with maximum aggregate size of 10 mm. All specimens were cast and cured in a horizontal position for 28 days. The targeted 28-day concrete compressive strength was C30/37 with the actual cube concrete compressive strength taken from testing 18 cubes according to BS EN 12390-3 [26] and shown in Table 1.

Two types of longitudinal reinforcement bars were used in this study: reinforcing steel bars grade 500 according to BS4449 [27] and GFRP bent bars made with polyester resin and E-Glass. All stirrups used were $\varnothing 4$ mm diameter mild steel according to BS EN 10277 [28]. The anchorage of the steel bars was done by using 90-degree hooks. For the steel rebars, the bent was done in the laboratory while for the GFRP, it was done by the manufacturer in the factory during the production process. Material tests were conducted on eight reinforcing rebars according to BS EN ISO 6892-1:2019 [29] with the standard deviation of 15.1. Five GFRP bars were tested by the manufacturer and the obtained mechanical properties are shown in Table 3.

3.3. Test setup, instrumentation and procedure

The test set up for all tested specimens is showed in Fig. 2. The samples were bolted to the strong reaction frame with the anchorage bolts from the RC foundation. The cyclic lateral load was applied at the beam level in the in-plane horizontal direction by using a screw jack, electric motor and inverter. The centreline of the beam was aligned with the centreline of the actuator. Vertical load on the frames is not taken into consideration as one of possible scenarios of loading, such as top floor or single floor building. High strength threaded bars were used along the middle longitudinal axis of the beam for the pushing and pulling loading mechanism. The actuator was programmed by the data acquisition system to apply the cyclic loading in both directions in a displacement-controlled mode. The rate of applying the displacement was different for small and large amplitudes. Thus, for the initial drifts up to 0.75% (or 5.8 mm displacement) the rate was 1 mm/min and around 3 mm/min thereafter for larger amplitudes.

The loading protocol, illustrated in Fig. 3, was based on ACI-374.1:05 [30] acceptance criteria and consisted of one displacement-controlled phase. During this phase, three identical reversed cycles were applied at each drift ratio. The drift ratio was calculated as the ratio between the horizontal displacement of the cross point between column centreline and the beam centreline. The column height was measured from the point of load application down to the

Table 3

Mechanical properties of the reinforcement.

Bar type	Bar diameter (mm)	Modulus of elasticity (GPa)	Tensile Strength (MPa)	Yield Strength (MPa)	Yield /ultimate strain (%)
Steel	$\varnothing 4$	193 ^a	573 ^a	374 ^a	$\epsilon_y = 0.19$
Steel	$\varnothing 6$	204 ^a	629 ^a	472 ^a	$\epsilon_y = 0.23$
GFRP	$\varnothing 6$	47.81 ^a	1123.56 ^a	-	2.35

^a Experimental values

footing interface and was recorded as 770 mm. The first drift ratio of 0.2% was selected as to be within the linear elastic response range for the control sample. Subsequent drift ratios were established to be values not less than one and one-quarter times, and not more than one and one-half times, the previous drift ratio [30]. By following this arrangement, the displacements were increased gradually in steps that were neither too large nor too small.

A 500 kN capacity load cell was attached to the screw jack in order to monitor the load in real time. Eight linear variable displacement transducers (LVDTs) were placed at different places to measure the displacement of the specimens. Several electrical resistance strain gauges were bonded to the surface of the concrete and to the reinforcing bars at critical locations (at the top and bottom of columns and at the beam-column interface) to monitor and record the strains. Crack formation and propagation on concrete was observed and marked out at the end of each drift step for both positive (pushing) and negative (pulling) directions. Photos of the specimens were taken at each amplitude. The tests were stopped after the load dropped more than 64% as average for the G series (equipment limitations with maximum displacement of 45 mm) and more than 79% as average for the S series from the maximum load reached by each sample.

4. Test results and observations

4.1. General observations

The formation and propagation of cracks was marked at the maximum displacement in both directions at each cycle for every drift. The main damage was localized at the column-beam interface and bottom region of the columns and was indicated by flexure and shear cracking. In general, the formation of cracks was symmetrical until the maximum load was reached and they were concentrated at the beam ends as well as column bases. As expected, the failure mode of the control specimens was concrete crushing followed by bars rupture. For specimens reinforced with GFRP bars, the destruction occurred more gradually and at later drifts with spalling and crushing of the concrete followed by rupture of reinforcement. Fig. 4 shows the condition of the specimens at the point of failure.

4.2. Hysteretic behaviour (lateral load-drift response) and maximum loads

The hysteretic behaviour for all tested specimens is presented in Fig. 5 in terms of lateral load – drift relationship. The load-drift envelope is indicated on the hysteretic loops with a red dashed line. The test results for all specimens indicate a stable hysteretic behaviour up to maximum capacity, followed by a gradual strength degradation.

The hysteretic loops were comparatively wider for the control specimens than for their counterparts which resulted in larger energy dissipation at the initial stages.

In Series 1, both specimens, S1 from Fig. 5(a) and G1 from Fig. 5(b), showed almost symmetric responses in pushing and pulling directions.

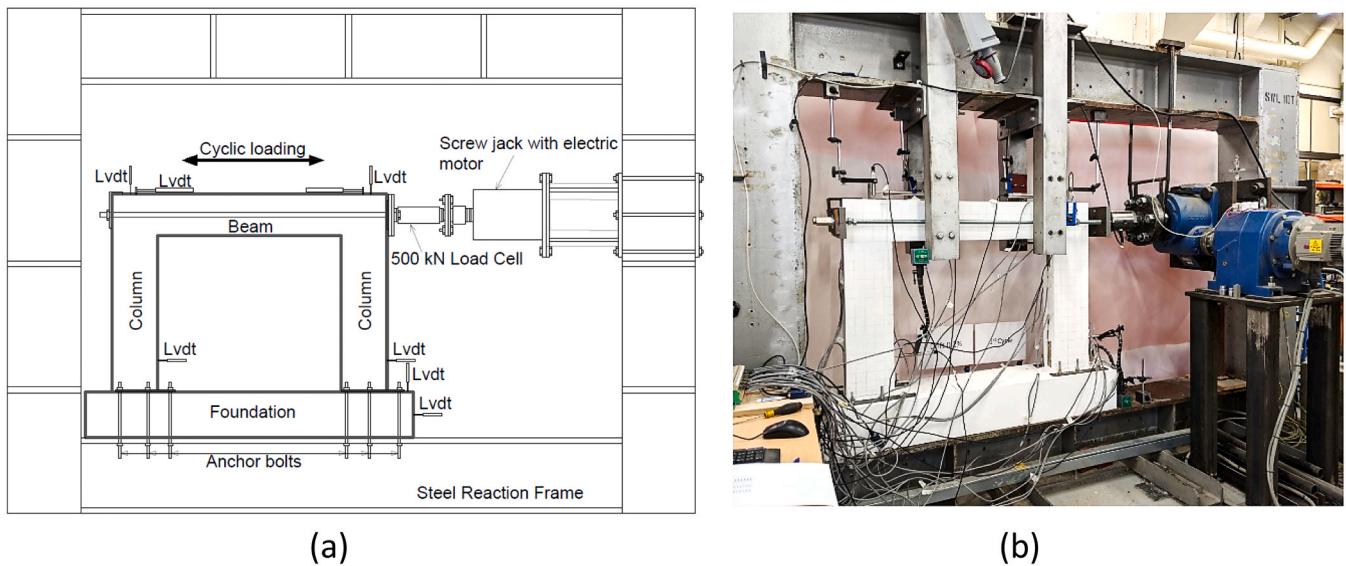


Fig. 2. Test set up: (a) schematic drawing of set up, (b) photo of set up.

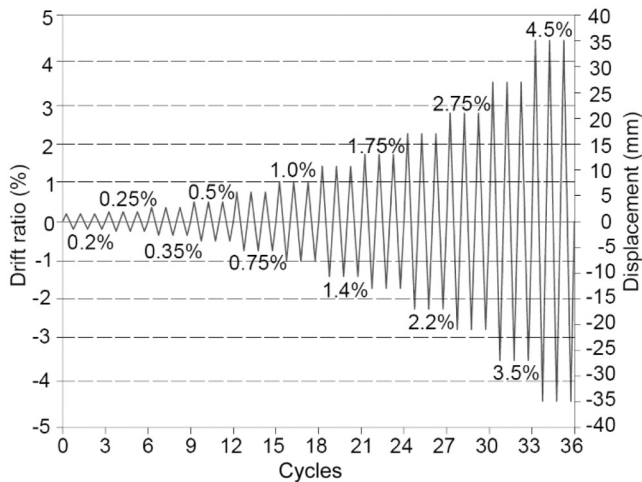


Fig. 3. Loading history.

The crack formation and propagation were almost symmetrical in pushing and pulling directions for each specimen. S1 reached the maximum load of 71 kN in pushing direction and 68 kN in pulling at 1.75% drift (13.5 mm) and 2.20% (16.9 mm) respectively. The specimen exhibited lower resistance in pulling than in pushing at maximum load with a difference of 3 kN. The maximum drift was reached by the specimen at 4.2% (32 mm) in pushing and at 4.3% (33 mm) in pulling direction, associated with a drop in load of 56% and 76% from the maximum load in pushing and pulling directions. By comparison, G1 reached a maximum load of 70 kN at 3.3% drift (25 mm) in pushing and 64 kN at 3.4% drift (26 mm) in pulling. This indicated that the G1 carried 3.6% less load than the control sample. The specimen exhibited lower resistance in pulling than in pushing at maximum load with a difference of 6 kN. The maximum drift reached was at 5.20% (40 mm) in both directions corresponding to a drop in load of 55% and 75% respectively from pushing and pulling directions. As expected, the graph indicates that the G1 frame had initial narrower loops than the S1 frame which resulted in lower energy dissipated at initial drifts.

A summary of these experimental values for the frames is presented in Table 4. The maximum load achieved by each frame is presented in pushing and pulling directions with their corresponding drifts.

Similarly, the maximum drift in both directions is shown together with the associated load drop. This load in percentage, was calculated from the maximum load achieved by the frames and the load at maximum drift.

In Series 2, specimen S2 in Fig. 5(c) reached the maximum load of 51 kN in pushing direction and 48 kN in pulling at 1.75% drift. At the maximum load achieved, the specimen exhibited lower resistance in pulling than in pushing with a difference of 3 kN. The maximum drift was reached at 4.5% (35 mm) in both directions corresponding to a drop in load of 87% and 97% from pushing and pulling. The specimen G2, Fig. 5(d), reached a maximum load of 42 kN at 2.74% drift (21 mm) in pushing and 46 kN at 3.5% drift (27 mm) in pulling. Compared to the control sample, this specimen showed 11.1% less lateral capacity. The specimen exhibited higher resistance in pulling than in pushing at maximum load with a difference of 4 kN. The maximum drift reached was at 5.8% (45 mm) in both directions corresponding to a drop in load of 68% and 77% from pushing and pulling.

In Series 3, specimen S3 in Fig. 5(e) reached the maximum load of 56 kN in pushing direction and 58 kN in pulling at 1.4% drift (10.7 mm). The specimen exhibited higher resistance in pulling than in pushing at maximum load with a difference of 2 kN. The maximum drift was reached at 2.74% (21 mm) in both directions corresponding to a drop in load of 74% and 95% from pushing and pulling directions, respectively. Specimen G3 in Fig. 5(f) reached a maximum load of 61 kN in pushing and 58 kN in pulling at the same drift of 2.74% which is with 4.2% higher than its counterpart. At maximum load, the specimen exhibited lower resistance in pulling than in pushing with only 3 kN difference. The maximum drift reached was at 5.2% (40 mm) in both directions corresponding to a drop in load of 81% and 79% from pushing and pulling.

A summary of the maximum amplitude achieved by the frames in this study is presented in Table 5. The corresponding load in both directions is also shown along with the total number of cycles.

The maximum load achieved by each sample from either pulling or pushing is compared in Fig. 6.

The design lateral capacity of the reinforced concrete frames was determined by considering the plastic moments at the top and base sections of the columns. In the mechanism of the frames S1, S2 and S3, assuming that plastic hinges occurred at the bottom and top of the columns, the flexural capacity of the frames was calculated using the following expression:

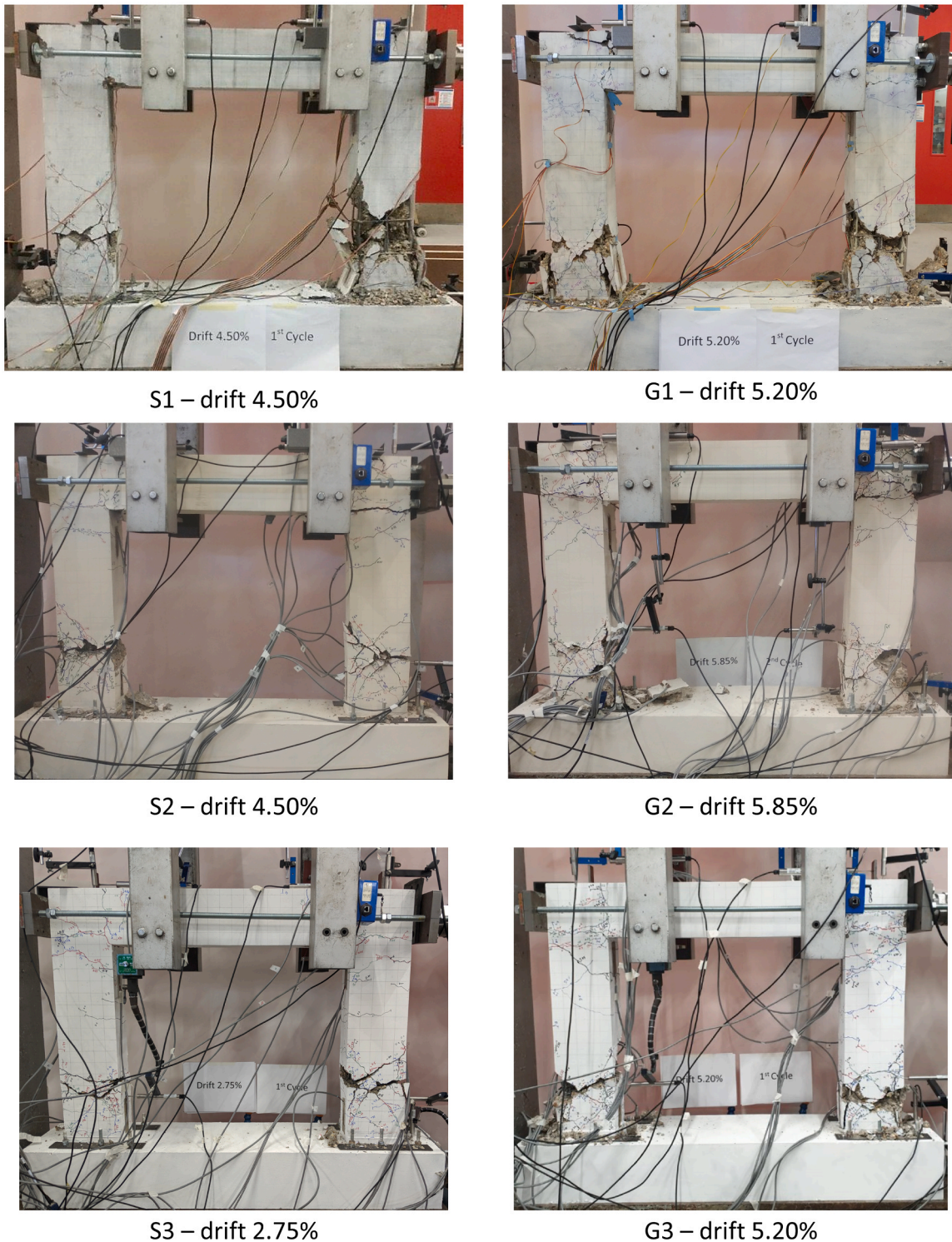


Fig. 4. Condition of tested samples at final drifts.

$$F_f = \frac{4M_p}{H}$$

where M_p = plastic moment of the column calculated from plastic analysis of the sections, H = clear height of the column, which was 680 mm. The axial load was taken as 0. The analytical calculations and experimental values of reinforced concrete frames are summarized in Table 6. It could be seen that S1 and S3 reached and exceeded their design capacity, while S2 had 1 kN less capacity than in design.

4.3. Envelope curves and stiffness degradation

The envelope curves are presented in Fig. 7(a) (b)(c) as lateral load-drift relationship which are showed as the maximum load from the positive and negative direction of the first cycle of each amplitude. In the first two series, the S specimens had higher lateral load capacity than the G specimens, but in the last series, G3 had a slightly higher load capacity than its steel counterpart. Since the compressive strength of the concrete was the same, this load increase could be attributed to the steel stirrups

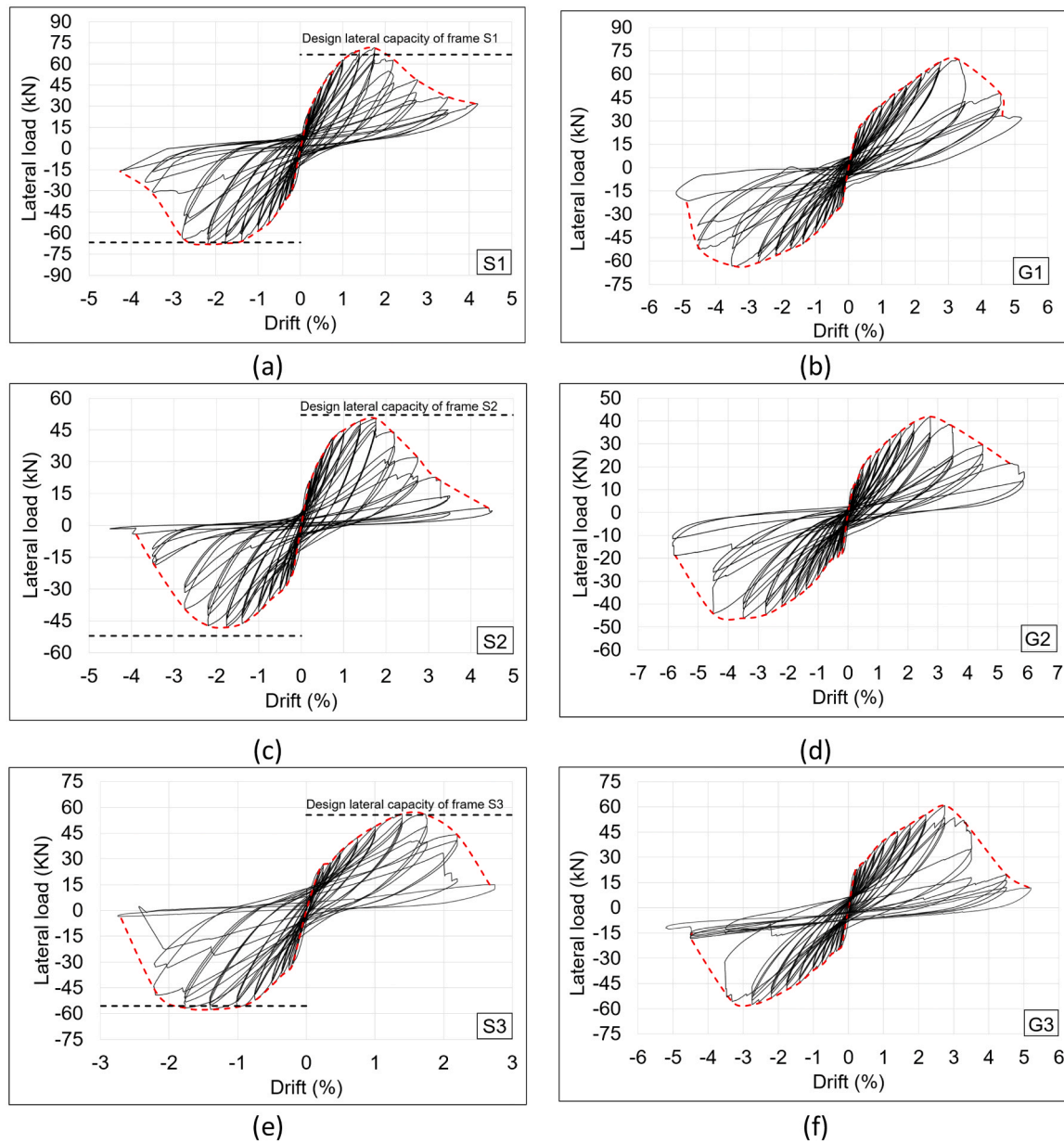


Fig. 5. Hysteresis loops of tested specimens: (a) specimen S1, (b) specimen G1 (c) specimen S2, (d) specimen G2, (e) specimen S3, (f) specimen G3.

Table 4

Summary of the experimental values for the frames.

Frame	Max load pushing [kN]	Corresponding drift pushing [%]	Max load pulling [kN]	Corresponding drift pulling [%]	Max drift achieved by the frame pushing / pulling [%]	Associated load drop pushing / pulling [%]
S1	71	1.75%	68	2.2%	4.2% / 4.3%	56% / 76%
G1	70	3.3%	64	3.4%	5.2% / 5.2%	55% / 75%
S2	51	1.75%	48	1.75%	4.5% / 4.5%	87% / 97%
G2	42	2.74%	46	3.5%	5.8% / 5.8%	68% / 77%
S3	56	1.4%	58	1.4%	2.74% / 2.74%	74% / 95%
G3	61	2.74%	58	2.74%	5.2% / 5.2%	81% / 79%

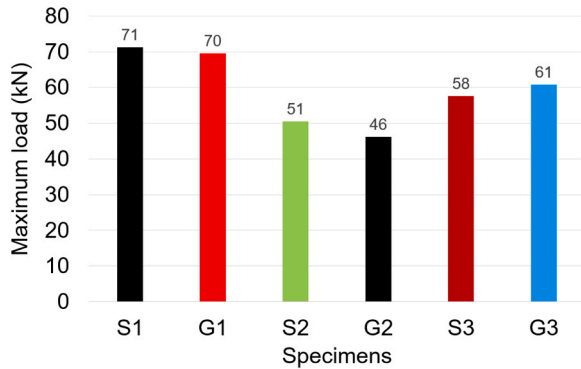
which appeared to have a more significant influence in improving the capacity of the frame for the G3 sample than for the S3 sample. Generally, the S series showed a higher initial stiffness than the G series, which was also reported by other researchers [31], due to the higher modulus of elasticity of steel compared to GFRP. This lower modulus of

elasticity of GFRP bars resulted in lower initial stiffness of the G series but increased the lateral displacement of the frames. It was also noticed that, after the peak load was reached, the S series exhibited a sudden drop in lateral load while the degradation in capacity of the G series was more gradual.

Table 5

Summary of the maximum amplitudes achieved by the frames.

Frame	Total no of cycles	Amplitude in pushing (mm)	Corresponding Load in pushing (kN)	Amplitude in pulling (mm)	Corresponding Load in pulling (kN)
S1	34	32	31	33	16
G1	37	40	31	40	16
S2	34	35	7	35	2
G2	38	45	13	45	10
S3	28	21	15	21	3
G3	37	40	11	40	12

**Fig. 6.** Comparison of maximum loads achieved by each sample.**Table 6**

Analytical calculations and experimental values of reinforced concrete frames.

	Plastic moment of column, M_p (kN*m)	Analytical frame strength, F_f (kN)	Experimental frame strength, $F_{f,exp}$ (kN)	Strength ratio, $F_{f,exp} / F_f$
S1	11.33	66.66	71.00	1.07
S2	8.86	52.12	51.00	0.98
S3	9.45	55.59	58.00	1.04

The maximum average load from pushing and pulling directions at different drifts is showed in Fig. 7(d)(e)(f); it was calculated as the average of the maximum load from positive and negative directions from the 1st cycle at each amplitude. It could be observed that the S series reached their ultimate loads at earlier drifts than the G series which withstood loads at higher drift ratios. The reinforcement ratio in the columns had a direct effect on the ultimate capacity of the specimens. A direct comparison of this parameter could be made between Series 1 and Series 3. The first Series 1 (S1, G1), which was reinforced with 8 bars, had greater capacity than Series 2 and 3 (S2, G2, S3, G3) which had only 6 bars. It was also observed that the presence of steel links in the joints for the 3rd series had a significant impact on the behaviour of the samples, increasing the shear strength of the joints and thus the capacity of the specimens. The 3rd series had a bigger maximum load carrying capacity than the 2nd series as it could be seen from the 31% increase in load in G3 compared with G2 and only 12% increase in S3 compared with S2. As G3 achieved higher load capacity than S3, it is important to notice that the added steel stirrups in the joints had a more beneficial contribution to the overall frame capacity of the G3 than of the S3 specimen.

The differences between S and G specimens are captured in Fig. 7(g). The data is computed from the average load/drift graph presented earlier. As already seen from previous graphs, the S specimens showed higher initial stiffness than the G specimens as well as slightly higher load carrying capacity than their counterparts. As this was achieved at earlier drifts, it can be noticed that when the G specimens reached their peak load at 2.75% drift, the load of the S specimens had dropped 42% from their maximum load achieved in the experiment. This is due to the

fact that the G specimens underwent bigger displacements (up to 5.7% drift) than the S specimens (up to 4.5%).

The stiffness degradation over the drift for each sample is presented in Fig. 8(a)(b)(c) by comparing the specimens within each series. The secant stiffness is defined as the slope of the line between the peak loads from the envelope curves graph. The peak-to-peak stiffness was then calculated as the ratio of the sum of the peak loads from positive and negative direction for each target amplitude over the sum of the corresponding drift. It can be noticed that the stiffness of all specimens decreased gradually as the drift increased and all of them experienced severe degradation by the end of the experiment. As expected, the initial stiffness of GFRP reinforced specimens was lower than the initial stiffness of their counterparts for the same series which is in accordance with the findings of other researchers. This is due to the higher modulus of elasticity of steel (204 GPa) compared to the one of the GFRP bars (47 GPa). At the initial drift of 0.20%, S1 had 24% more stiffness than G1; S2 had 30% more stiffness than G2; S3 had 18% more stiffness than G3. The largest difference between the specimens was noticed at a same drift of 0.5% for all series; so, S1 had 32% more stiffness than G1, S2 had 37% more than G2 and S3 had 28% more than G3. However, at the final drifts, the G frames had more stiffness than the S frames. Consequently, at 4.5% drift, G1 and G2 had 48% and 81% more stiffness than S1 and S2; at 2.75% drift, G3 had 83% more stiffness than S3.

A similar pattern in stiffness degradation could also be observed from the average stiffness of the G series and S series from Fig. 8(d); for instance, at 1% drift, the average stiffness of the S series was 31% higher than that of the G series. However, at 2.20% drift and progressing until the final drifts, the GFRP specimens exhibited higher stiffness than the control ones. This could be attributed to the steep degradation of the S series caused by the yielding of the steel. At 3.5% drift, the average stiffness of the G series was 48% higher than their counterparts.

The residual displacement after various drift levels for the GFRP-reinforced frames and their RC counterpart is shown in Fig. 9.

The residual displacement at each drift is found when the load is reaching zero after a whole first cycle. It is evident from the graph that, in all three series, the GFRP-reinforced frames exhibited a much lower residual displacement than their counterparts. This is a good indication that, in a seismic event, the damage induced to the GFRP frames at the same level of drift is lower than to the RC frames. Similar findings were also reported by other researchers [19].

4.4. Cumulative energy dissipation

A comparison of the cumulative energy dissipated for all tested samples is presented in Fig. 9(a). The cumulative energy dissipated was calculated by summation of the enclosed area in the hysteretic loops in successive load-displacement cycles. For each cycle, the energy dissipation was calculated as the area that the loop encloses in that particular load displacement graph. Generally, the S series dissipated energy through larger hysteric loops than the G series at the first drifts. The energy dissipation capacity of the frames was directly influenced by the reinforcement ratio in the columns and so the first group (S1, G1) resulted in higher values than the rest of the groups at the final drifts. The biggest difference between the specimens was recorded at 1.75% drift at which S1 exhibited 97%, S2 126% and S3 74% more cumulative

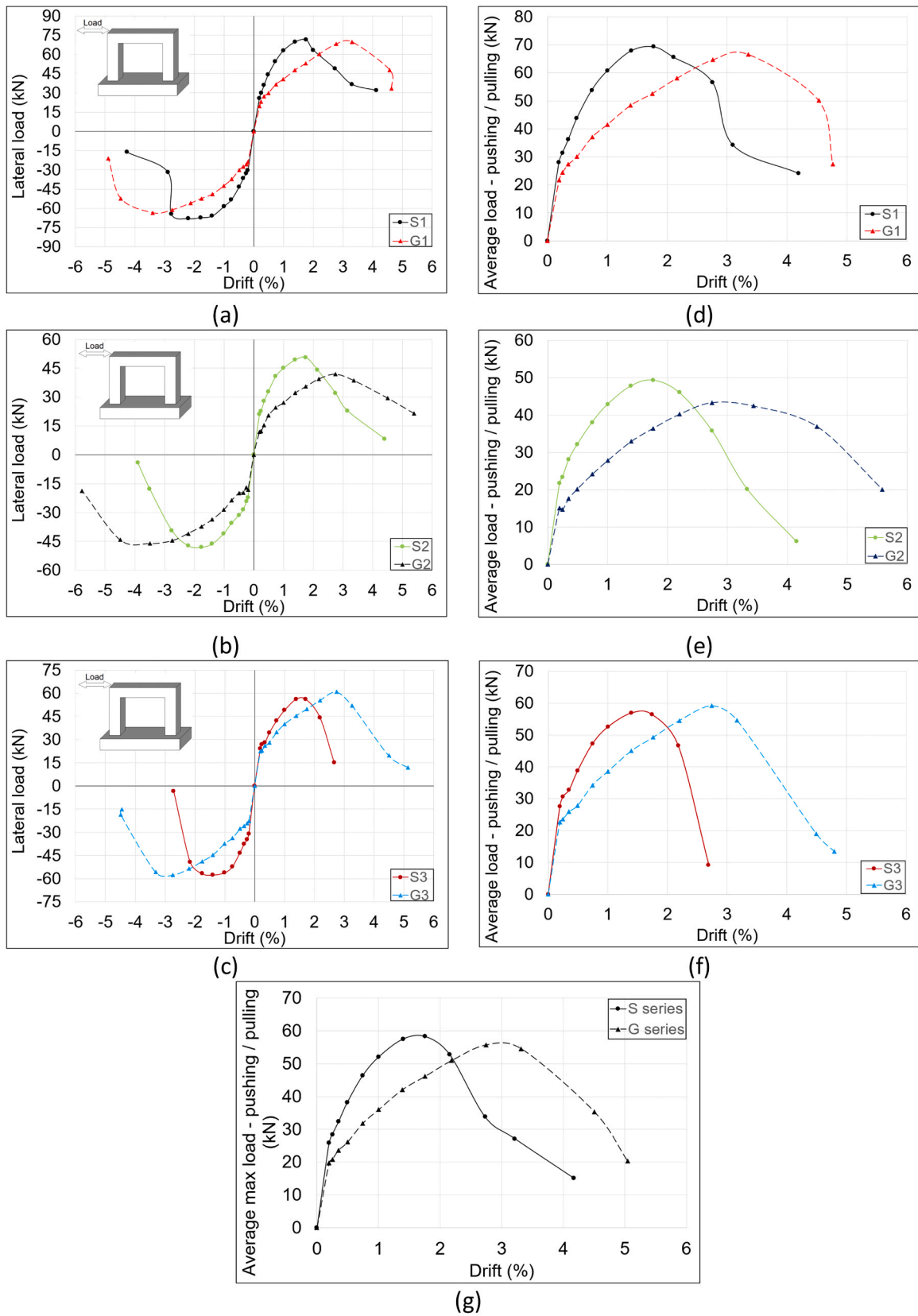


Fig. 7. (a)(b)(c) Envelope Curves, (d)(e)(f) average peak load from pushing and pulling cycles, (g) average peak load from S and G series.

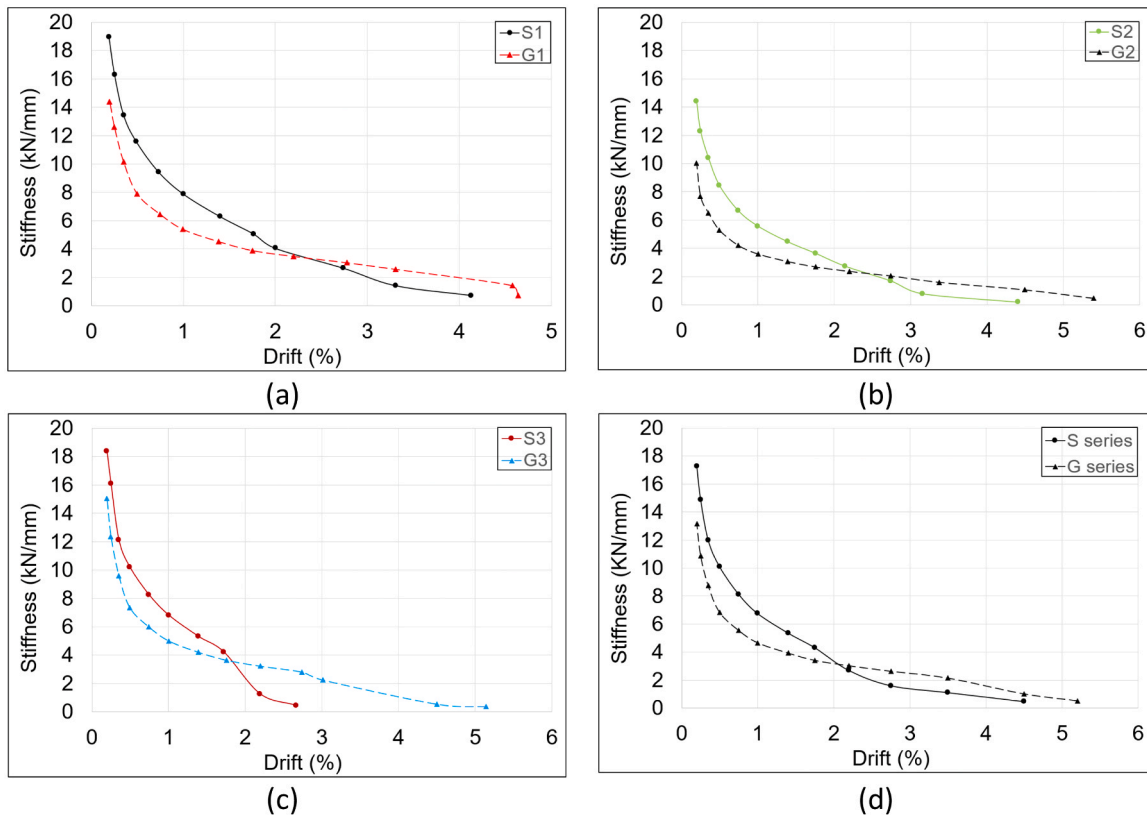


Fig. 8. (a)(b)(c) Stiffness Degradation, (d) average stiffness degradation from the S and G series.

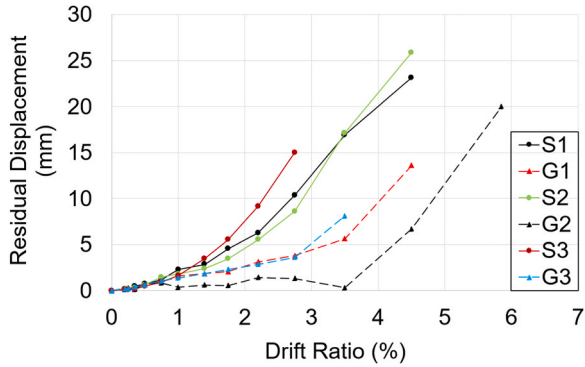


Fig. 9. Residual Displacement for all tested frames.

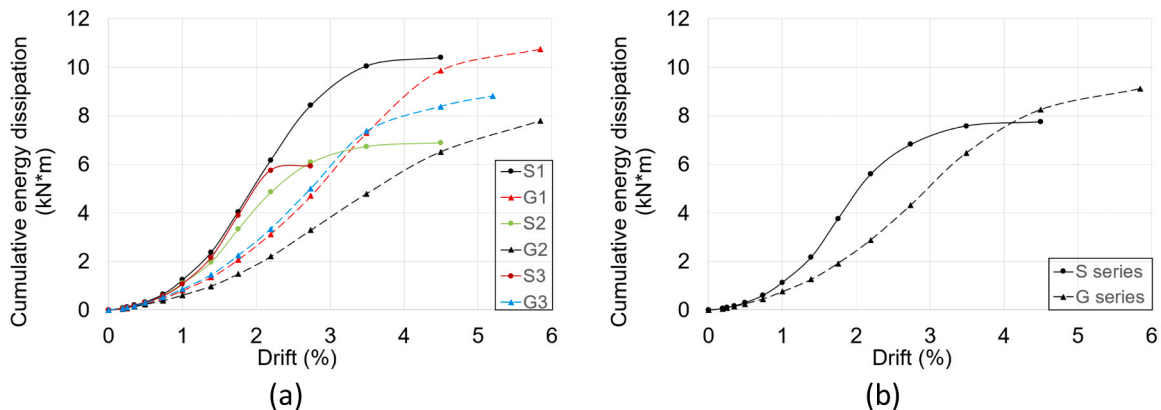


Fig. 10. Cumulative energy dissipation: (a) all tested samples, (b) average S and G series.

energy dissipated compared with the GFRP counterparts. However, at the final drifts, the G1, G2, and G3 specimens recorded 3%, 12% and 33% more energy dissipation than S1, S2 and S3 respectively.

Another factor influencing the energy dissipation capacity of the frames was the presence of the stirrups at the joints. The highest impact was observed for the G3 specimen as the stirrups actively participated in the energy capacity of the frame and enhanced it considerably. Consequently, even though G1 had higher reinforcement ratio in the columns and showed higher lateral load capacity than G3, the latter indicated greater energy dissipation than G1 up to 3.5% drift.

The average cumulative energy dissipated between the S and G specimens is summarised in Fig. 9(b). The maximum difference between them was highlighted at 1.75% drift, where the average cumulative energy dissipated of the S specimens is 49% higher than that of the G specimens. With the increase in drift, the difference between them decreases so that by the end of the experiments the cumulative energy

dissipated of the G series is 15% greater than that of the S series. This could be attributed to their ability to undergo large displacement as seen earlier.

In this experimental study, three GFRP reinforced concrete frames were investigated under reversed cyclic loading and compared with steel reinforced concrete frames. As no vertical load was considered on the beams or columns, the presented results are with limited applicability and could be used for comparison for further research. The effect of vertical loads on the frame could have an impact in the damage evolution of the specimens resulting in a change in stiffness and energy dissipation.

5. Conclusions

This paper presented some results from a research program which deals with the investigation of GFRP bars as main reinforcement in concrete frames. The experimental investigation of concrete frames reinforced with steel (S series) and GFRP bars (G series) under reversed cyclic loading indicated a range of similarities and differences. Based on the results obtained from the testing of six 1/3 scale down frames, the following conclusions can be made:

- The S samples showed a higher initial stiffness than the G samples, while the G samples exhibited higher stiffness from 2.20% drift onwards.
- The average stiffness from the G samples at 3.5% drift was 48% more than their counterparts.
- The G frames had approximately the same load bearing capacity as the S frames.
- The G frames reached their ultimate loads at higher level of displacement than their counterparts.
- The G frames exhibited a much lower residual displacement than the S frames
- When the G frames reached their peak load at 2.75% drift, the load of the S specimens had dropped 42% from their maximum load achieved.
- After the peak load was reached, the S samples exhibited a sudden drop in load while for the G samples it was a more gradual degradation in capacity.
- Series 1 (for both S and G samples) had greater ultimate load capacity than Series 2 and 3 due to higher reinforcement ratio in the columns.
- The ultimate capacity for the G3 was higher than the S3
- The S samples dissipated energy through wider hysteretic loops than the G samples at the first drifts; at 1.75% drift, the average cumulative energy dissipated of the S specimens was 49% higher than the G specimens; at 5.8% drift, G1, G2, and G3 recorded 3%, 12% and 33% more cumulative energy dissipation than S1, S2 and S3 respectively.

In summary, the conducted experiments indicate that GFRP reinforced frames (G series) can develop approximately the same loading capacity as the control frame (S series), with the indication that the ultimate values of load appeared to be at higher displacement. Although no vertical load was considered on the frames in this study, during an earthquake event, the behaviour of a GFRP reinforced frame could allow bigger displacements than the conventional RC frames before reaching ultimate load values, this way allowing for better distribution of stresses and higher energy dissipation before destruction.

Recommendations for further research

Recommendations for further research on GFRP-reinforced frames:

- To investigate the effect of vertical loads on the frames.
- To investigate the behaviour of frames with infill.

CRedit authorship contribution statement

Donchev Ted: Writing – review & editing, Supervision. **Petkova Diana:** Writing – review & editing, Supervision. **Georgopoulos Costas:** Supervision, Investigation. **Limbachiya Mukesh:** Supervision. **Hopartean George:** Writing – review & editing, Writing – original draft, Project administration, Methodology, Investigation, Formal analysis, Data curation.

Declaration of Competing Interest

The authors declare that they have no known competing financial interests or personal relationships that could have appeared to influence the work reported in this paper.

Data Availability

Data will be made available on request.

Acknowledgments

The authors would like to express their gratitude for the bent GFRP bars provided by ATP construction composites, Italy. This research did not receive any specific grant from funding agencies in the public, commercial or non-for-profit sectors.

References

- [1] Micelli F, Nanni A. Durability of FRP rods for concrete structures. *Constr Build Mater* 2004;18:491–503. <https://doi.org/10.1016/j.conbuildmat.2004.04.012>.
- [2] Bakis CE, Bank LC, Asce F, Brown VL, Asce M, Cosenza E, et al. Fiber-reinforced polymer composites for construction- state-of-the-art review. *J Compos Constr* 2002;6:73–7.
- [3] Mufti P, Onofrei AA, Benmokrane M, Banthia B, Boulfiza N, Newhook M, et al. Field study of glass-fibre-reinforced polymer durability in concrete1. *Can J Civ Eng* 2007;34:355.
- [4] Nanni A, De Luca A, Zadeh H. *Reinforced Concrete with FRP Bars: Mechanics and Design*. CRC Press, Taylor & Francis Group; 2014.
- [5] Ruiz Empanaza A, Kampmann R, De Caso F, Morales C, Nanni A. Durability assessment of GFRP rebars in marine environments. *Constr Build Mater* 2022;329:127028. <https://doi.org/10.1016/j.conbuildmat.2022.127028>.
- [6] Hollaway LC. A review of the present and future utilisation of FRP composites in the civil infrastructure with reference to their important in-service properties. *Constr Build Mater* 2010;24:2419–45.
- [7] T. Uomoto, H. Mutsuyoshi, F. Katsuki, S. Misra, Use of Fiber Reinforced Polymer Composites as Reinforcing Material for Concrete, 14 (2002) 191–209.
- [8] B. Benmokrane, H. Mohamed, E. Ahmed, Recent developments of FRP bars as internal reinforcement in concrete structures & field applications, *Sustain. Constr. Mater. Technol.* 2016-August (2016).
- [9] fib, FRP Reinforcement in RC Structures, Bulletin 40, International Federation for Structural Concrete (fib), Lausanne, Switzerland, 2007.
- [10] A.C.I. CODE-440.11–22: Building Code Requirements for Structural Concrete Reinforced with Glass Fiber-Reinforced Polymer (GFRP) Bars—Code and Commentary, 2023.
- [11] fib. Model Code 2010. Bulletins Nos. 65/66, Federation Internationale du Beton: Lausanne, 2012.
- [12] ACI 440.1R-15 Guide for the Design and Construction of Structural Concrete Reinforced with Fiber-Reinforced Polymer (FRP) Bars, American Concrete Institute, Farmington Hills, MI 48331, 2015.
- [13] M. Fukuyama, H., Masuda, Y., Sonobe, Y., and Tanigaki, Structural performances of concrete frame reinforced with FRP reinforcement, in: 2nd Int. RILEM Symp. Non-Metallic Reinf. Concr. Struct., Ghent, Belgium, 1995: pp. 275–286.
- [14] Said AM, Nehdi ML. Use of FRP for RC frames in seismic zones: part II. Performance of steel-free GFRP-reinforced beam-column joints. *Appl Compos Mater* 2004;11:227–45.
- [15] Mady Mohamed, El-Ragaby Amr, El-Salakawy Ehab. Seismic behavior of beam-column joints reinforced with GFRP bars and stirrups. *J Compos Constr ASCE* 2011.
- [16] Kazem Sharbatdar M, Saatcioglu M, Benmokrane B. Seismic flexural behavior of concrete connections reinforced with CFRP bars and grids. *Compos Struct* 2011;93:2439–49.
- [17] Hasaballa Mohamed, El-Salakawy Ehab. Shear capacity of exterior beam-column joints reinforced with GFRP bars and stirrups. *J Compos Constr ASCE* 2016;20.
- [18] Ghomi Shervin K, El-Salakawy Ehab. Seismic behavior of exterior GFRP-RC beam–column connections: analytical study. *J Compos Constr ASCE* 2018;22.
- [19] Ghomi Shervin K, El-Salakawy EF. Cyclic behavior of glass fiber-reinforced polymer-reinforced concrete exterior beam-column-slab connections. *Acids Struct J* 2020;117:171–83.

- [20] Ghomi SK, El-Salakawy E. Effect of joint shear stress on seismic behaviour of interior GFRP-RC beam-column joints. *Eng Struct* 2019;191:583–97. <https://doi.org/10.1016/j.engstruct.2019.04.091>.
- [21] Aliasghar-Mamaghani Mojtaba, Khaloo Alireza. Seismic behavior of concrete moment frame reinforced with GFRP bars. *Compos Part B Eng* 2019;163:324–38.
- [22] Hasaballa M, El-Salakawy E. Anchorage performance of GFRP headed and bent bars in beam-column joints subjected to seismic loading. *ASCE, J Compos Constr* 2018.
- [23] El-Mandouh MA, Omar MS, Elnaggar MA, Abd El-Maula AS. Cyclic behavior of high-strength lightweight concrete exterior beam-column connections reinforced with GFRP. *Buildings* 2022;12:1–26. <https://doi.org/10.3390/buildings12020179>.
- [24] BSI. (2014). BS EN 1992–1-1: 2004+ A1: 2014. Eurocode 2: Design of concrete structures. General rules and rules for buildings (incorporating corrigenda January 2008, November 2010 and January 2014), Civ. Eng. 144 (2001) 23–28.
- [25] EN, B. (2004). 1: 2004+ A1: 2013 Eurocode 8: Design of structures for earthquake resistance. General rules, seismic actions and rules for buildings, 1998–1., 3 (2004).
- [26] BS EN 12390–3:2019 Testing hardened concrete Part 3: Compressive strength of test specimens, (2019).
- [27] BS 4449:2005+A3:2016 Steel for the reinforcement of concrete. Weldable reinforcing steel. Bar, coil and decoiled product. Specification, (2016).
- [28] BS EN 10277:2018 Bright steel products. Technical delivery conditions, (2018).
- [29] BS EN ISO 6892–1:2019 Metallic materials — Tensile testing, Part 1: Method of test at room temperature, (2019).
- [30] ACI Committee 374, Acceptance Criteria for Moment Frames Based on Structural Testing and Commentary, ACI-374.1:05, Farmington Hills, MI 48331, 2014.
- [31] Sheikh SA, Kharal Z. Replacement of steel with GFRP for sustainable reinforced concrete. *Constr Build Mater J* 2018;160:767–74.